Autonomous Calibration of MEMS Gyros in Consumer Portable Devices

You Li, *Student Member, IEEE*, Jacques Georgy, *Member, IEEE*, Xiaoji Niu, Qingli Li, and Naser El-Sheimy

***Abstract*— This paper presents a real-time calibration method for gyro sensors in consumer portable devices. The calibration happens automatically without the need for external equipment or user intervention. Multilevel constraints, including the pseudoobservations, the accelerometer and magnetometer measurements, and the quasi-static attitude updates, are used to make the method reliable and accurate under natural user motions. Walking tests with the Samsung Galaxy S3 and S4 smartphones showed that the method provided promising calibration results even under challenging motion modes, such as dangling and pocket, and in challenging indoor environments with frequent magnetic interferences.**

***Index Terms*— MEMS sensors, IMU, smartphones, indoor navigation.**

I. Introduction

ADVANCES in Micro-Electro-Mechanical Systems (MEMS) technology combined with the miniaturization of electronics have made it possible to produce chip-based sensors, such as inertial sensors (i.e., accelerometers and gyroscopes (gyros)) and magnetometers. MEMS chips are small and lightweight, consume very little power, and are extremely low-cost [1]. By virtue of these advantages, MEMS sensors have become appropriate candidates for motion tracking and navigation (i.e., determination of attitude, velocity, and position) applications in many electronic devices such as smartphones, gaming systems, toys, and the next generation wearable devices. For consumer portable devices, dead reckoning (DR) is usually the navigation algorithm used to navigate with inertial sensors; thus, the sensors are not dependent on the transmission or reception of signals from an external source [2]. Such self-contained MEMS-based inertial sensors are ideal for providing continuous information for indoor/outdoor navigation [3].

TABLE I
PERFORMANCE OF TYPICAL MEMS SENSORS [5] IN SMARTPHONES

Sensor	Error	Range
Gyros	Initial Biases at 25 °C	± 5 deg/s
	Variation over -40 to 85 °C	± 0.24 deg/s/°C
Accelerom-eters	Initial Biases	± 60 mg
	Variation over -40 to 85 °C	± 0.64 mg/°C

However, low-cost MEMS inertial sensors suffer from significant run-to-run biases and thermal drifts [4]. The performance of typical MEMS sensors that used in smartphones [5] are shown in Table 1. Although lab calibration at room temperature is a useful way to remove many deterministic sensor errors [6], the sensors' readings can be very different due to the restart and the difference between the operational and calibration environments. Also, it is not affordable for the chip manufacturers to conduct thermal calibration of low-cost sensors. Due to the integration process in the inertial navigation mechanization, any sensor errors will accumulate, resulting in increasing navigation errors. For indoor environments, position or velocity updates from GNSS are not always available. If this is the case, the navigation accuracy will degrade faster over time.

Therefore, a real-time calibration process is needed to mitigate the drift of the inertial sensor errors, especially the gyro biases. The calibration process should happen automatically in the background without the need for user intervention. This is because mainstream consumer and non-professional users should be able to benefit from the calibration and from a better navigation solution using the calibrated sensors without any specific requirement from them. Achieving such a calibration is not easy, especially when working with consumer-grade inertial sensors. Most calibration methods require external equipment or tools to provide a reference for calibration. It is not realistic to expect the users of the electronic products to use a separate tool to calibrate the sensors. Furthermore, current traditional methods to calibrate the inertial sensors without an external tool involve: a) using static periods for gyroscopes calibration when the sensors are fully static; and b) using the gravity vector for accelerometer calibration while ensuring that the IMU covers various attitudes to make sure that the system is observable [7]. The need for static periods limits the scenarios where calibration can happen; the need for various attitudes increases the operation complexity.

Manuscript received December 10, 2014; revised January 21, 2015; accepted February 21, 2015. Date of publication March 16, 2015; date of current version May 20, 2015. The work of Y. Li was supported by the China Scholarship Council under Grant 201306270139. The work of X. Niu was supported by the National Natural Science Foundation of China under Grant 41174028 and Grant 41304004. The associate editor coordinating the review of this paper and approving it for publication was Prof. Kazuaki Sawada.

Y. Li is with the Department of Geomatics Engineering, University of Calgary, Calgary, AB T2N 1N4, Canada, and also with the GNSS Research Center, Wuhan University, Wuhan 430072, China (e-mail: liyou331@gmail.com).

J. Georgy is with InvenSense Inc., Calgary, AB T2L 2K7, Canada (e-mail: jgeorgy@invensense.com).

X. Niu and Q. Li are with the GNSS Research Center, Wuhan University, Wuhan 430072, China (e-mail: xjniu@whu.edu.cn; qlli@whu.edu.cn).

N. El-Sheimy is with the Department of Geomatics Engineering, University of Calgary, Calgary, AB T2N1N4, Canada (e-mail: elsheimy@ucalgary.ca).

Color versions of one or more of the figures in this paper are available online at http://ieeexplore.ieee.org.

Digital Object Identifier 10.1109/JSEN.2015.2410756

Furthermore, when the calibration is done automatically in the background, the need for various attitudes will delay having a full calibration without the user involvement to do specific motions.

In this paper, we propose an autonomous calibration method to calculate the gyros in consumer electronics. This method uses a Kalman filter algorithm and utilizes multiple constraints, including the pseudo-observations, the accelerometer and magnetometer measurements, and the quasi-static attitude updates. The advantages of the proposed calibration algorithm includes:

a) The calibration happens automatically without the need for external equipment or user intervention;
b) The algorithm works under natural user motions such as handheld, phoning, dangling, pocket, belt, and backpack. Also, there is no singularity problem when the pitch angle reaches $\pm$ 90°;
c) The algorithm works even in indoor environments with frequent magnetic interferences.

This paper is organized as follows. Section 2 reviews the previous relevant works. Section 3 explains the methodology of the calibration algorithm, including the details of multiple constraints. Section 4 shows some results with analysis and Section 5 draws the conclusion.

II. Previous Works

The commonly used calibration methods include the standard calibration methods [6], [8] and the multi-position calibration methods [7], [9]–[12]. Standard calibration methods determine sensor errors by comparing the sensor outputs with known reference inputs. Due to the dependence on specialized equipment, the standard methods are always designed for in-lab tests, factory calibration and relatively high-grade IMUs.

To calibrate an IMU just with simple devices or even without any specific tool, multi-position methods are developed. The basic idea of a multi-position method can be stated as follows: the norms of the measured outputs of the accelerometer and gyro cluster are equal to the magnitudes of the given specific force (i.e., gravity) and rotational velocity inputs (i.e., the Earth rotation), respectively [13]. However, the main drawback in using multi-position calibration method is that the gyro reference (the Earth rotation rate) is a weak signal (15 deg/h) which can result in observability problems. Therefore, a single axis turntable is required to provide a strong rotation rate signal [7], [10]–[12], which limits the multi-position method to laboratories.

To estimate gyro errors without any external equipment, an in-field calibration method has been developed [14]. The accelerometer triad is first calibrated by the multi-position method through multiple quasi-static states generated by hand holding. Then, the outputs from the calibrated accelerometers can be used to calibrate gyros. To avoid the requirement of being static/quasi-static, researches have presented gyro calibration methods such as the vertical gyro (VG) method [15] and the approach that uses accelerometers to estimate the horizontal gyro errors [16]. These methods are efficient in calibrating the horizontal gyros but have limited effect on the vertical gyro [16]. To make all sensor errors observable, user intervention is still required: the user needs to rotate the device to different attitudes to make sure that every gyro axis has the chance to experience the horizontal direction.

In this paper, we remove both the inconvenient user intervention process and the quasi-static assumption by using constraints from multiple sensors and apriori information. The features of the referred previous works and the proposed method are listed in Table 2.

III. Methodology

When compared with previous works, the main advantage of the proposed method is the removing of the requirement of equipment and user intervention. In addition, the proposed method can work in real time under natural human motions in both indoor and outdoor environments. In this section, the details of the proposed method will be given. We will also answer the following questions: a) how can the algorithm work under various human motions? and b) how can the algorithm work in indoor environments with frequent magnetic interferences?

Multi-level constraints are utilized to improve the calibration efficiency and accuracy. The first level is called pseudo-observation updates. This constraint is activated when the change in position between two time epochs is within a limited range. In this case, the constraints $\tilde{\mathrm{r}} = \text{constant}$ and $\tilde{\mathrm{v}} = 0$ are regarded as an observation of pseudo-position and pseudo-velocity. The uncertainty of position and velocity changes during the calibration process are embodied in the covariance matrix of measurement noise (R) in the Kalman Filter. The R matrix is tuned adaptively according to the IMU outputs. The use of the pseudo-observation updates makes it possible to calculate the gyro errors without external equipment or tools; also, the pseudo-observation updates can be used under natural human motions without special training. Therefore, it is feasible to run the calibration algorithm in the background without user interaction.

The second level of constraints is from accelerometers and magnetometers. We use the accelerometer and magnetometer measurements in a tightly-coupled way, which brings several benefits for the pedestrian navigation applications with various phone displacements. The details will be introduced later in this section.

Another advantage of our method is that it maximizes the contribution from magnetometers in environments with frequent magnetic perturbations. We make the magnetometer measurements reliable based on the following fact: to aid gyro calibration, what we need is attitude changes, instead of the absolute attitude. The proposed method can use the magnetometer measurements without knowing the absolute values of the local magnetic field (LMF) parameters (i.e., declination, inclination, and magnitude).

Moreover, the proposed calibration method is different from the traditional method which adds sensor errors into the navigation Kalman filter. The main objective of the navigation algorithm is to estimate the navigation states (i.e., position, velocity, and attitude) instead of sensor errors.

TABLE II
COMPREHENSIVE CHARACTERISTICS OF THE REFERRED PREVIOUS WORKS AND THE PROPOSED METHOD (IMPROVED BASED ON [16])

Method and author(s)	Required equipment	Calibration accuracy	Features
Standard methods (e.g. six-position method)	Specialized equipment	High	High precision and reliable
Multi-position method *(Lötters et al 1998)*	None (quasi-static required)	Low	Calibrate biases and scale factors of the tri-axial accelerometer under quasi-static conditions without any equipment
Improved multi-position methods *(Skog and Händel 2006, Syed et al 2007)*	A single axis angle turntable	High	Calibrate non-orthogonalities of tri-axial accelerometer as well; calibrate gyros using a single axis turntable
Improved multi-position method *(Zhang et al 2010)*	A single axis angle turntable	High	Detect the inter-triad misalignment between the accelerometer and gyro triads; Relax the requirement of precise orientation control.
Improved multi-position method *(Nieminen et al 2010)*	A single axis rate turntable	High	Exploiting the centripetal accelerations caused by the rotation of the turntable
Improved multi-position method *(Fong et al 2008)*	None (quasi-static required)	Low	Calibrate the low-cost gyro triad as well as accelerometers without any equipment
In-situ method *(Li et al 2012)*	None (in-situ required)	Low	Introduce pseudo-observations to calibrate the biases and scale factors of gyros and accelerometers without any equipment in a short period (about 30 seconds)
Proposed method	None	Low	Using Kalman filter algorithm with multi-level constraints to conduct calibration under natural user motions.

Therefore, when using extra apriori information or setting parameters, it is preferable to assure that any inaccurate estimate of sensor errors will not destroy the navigation algorithm rather than to estimate residual sensor errors with a higher accuracy. However, in the proposed calibration method, we use specific updates, such as the pseudo-observations, and set the Kalman filter parameters with the aim of maximizing the calibration accuracy. Also, the calibration results can be evaluated before feedback to avoid the degradation of the whole navigation system under extreme navigation conditions.

The algorithm is comprised of the IMU sensor error models, the INS mechanization, and the Kalman filter models. The INS mechanization follows [17] and will not be described in detail. For details about Kalman filter the reader can refer to [18]. The following sub-sections will introduce the algorithm, including system error models, the system model and the measurement model (for updates from multiple sensors and apriori information).

A. Sensor Error Models

A major problem of applying MEMS sensors is the changes of the biases and the scale factors [4]. With the current MEMS manufacturing technology, non-orthogonality errors are relatively smaller compared to the biases and scale factor errors. Therefore, only biases and scale factor errors are taken into account. The output error equations of accelerometers and gyros can be described respectively as below:

$$\delta \mathbf{f}^b = \mathbf{b}_a + diag(\tilde{\mathbf{f}}^b)\delta \mathbf{s}_a + \mathbf{w}_a \quad (1)$$

$$\delta \boldsymbol{\omega}_{ib}^b = \mathbf{b}_g + diag(\tilde{\boldsymbol{\omega}}_{ib}^b)\delta \mathbf{s}_g + \mathbf{w}_g \quad (2)$$

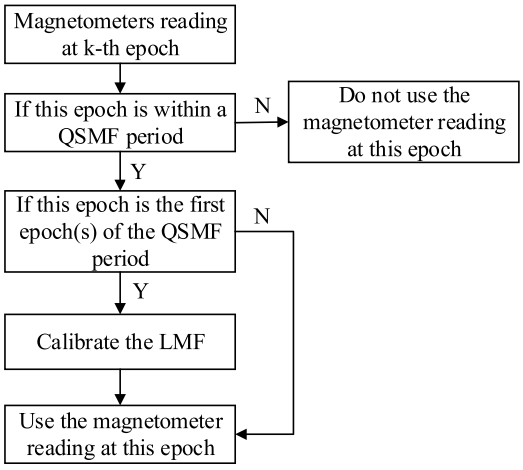

Fig. 1. The flowchart of using magnetometer data during QSMF periods.

where $\delta \mathbf{f}^b$ and $\delta \boldsymbol{\omega}_{ib}^b$ are the error vectors of specific force and angular rate, respectively. $\mathbf{b}_a$ and $\mathbf{b}_g$ are the accelerometer and gyro biases. $\delta \mathbf{s}_a$ and $\delta \mathbf{s}_g$ are the linear scale factor error vectors, $\mathbf{w}_a$ and $\mathbf{w}_g$ represent the sensor noises, and $\tilde{\mathbf{f}}^b$ and $\tilde{\boldsymbol{\omega}}_{ib}^b$ are the measured specific force and angular rate, respectively. The symbol $diag(\cdot)$ indicates the diagonal matrix form of a vector.

The sensor biases and scale factor errors are modeled as first-order Gauss-Markov processes [19]. Take the gyro biases as an example:

$$\dot{\mathbf{b}}_g = -(1/\tau_{bg})\mathbf{b}_g + \mathbf{w}_{bg} \quad (3)$$

where τ_{bg} denotes for the correlation time of the gyro biases and $\mathbf{w}_{bg}$ is the driving noise vector.

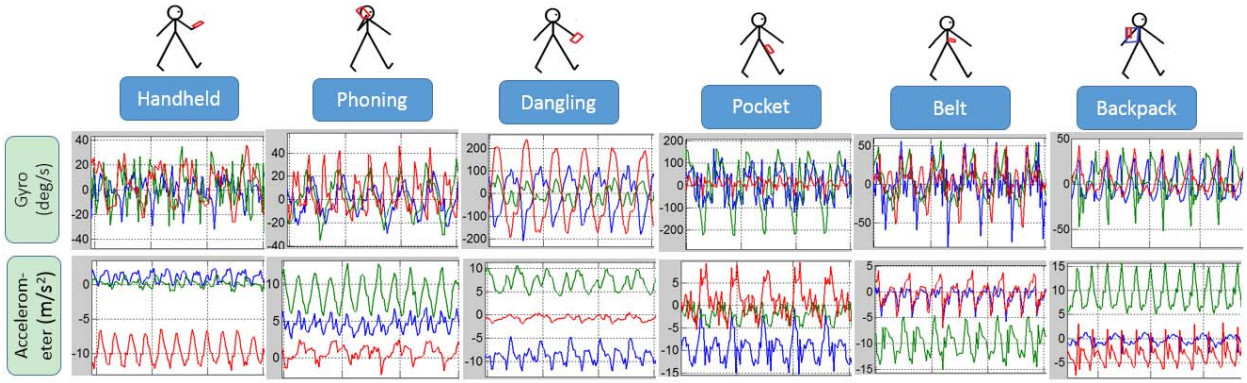

Fig. 2. Tested motion modes and corresponding gyro and accelerometer readings.

B. Kalman Filter-System Model

A simplified form of the psi-angle error model [17] is applied as the continuous-time state equations in the Kalman filter [16].

$$\begin{bmatrix} \delta\dot{\mathbf{r}}^n \\ \delta\dot{\mathbf{v}}^n \\ \dot{\boldsymbol{\psi}} \end{bmatrix} = \begin{bmatrix} -\boldsymbol{\omega}_{en}^n \times \delta\mathbf{r}^n + \delta\mathbf{v}^n \\ -(2\boldsymbol{\omega}_{ie}^n + \boldsymbol{\omega}_{en}^n) \times \delta\mathbf{v}^n + \mathbf{f}^n \times \boldsymbol{\psi} + \mathbf{C}_b^n \delta\mathbf{f}^b \\ -(\boldsymbol{\omega}_{ie}^n + \boldsymbol{\omega}_{ec}^n) \times \boldsymbol{\psi} - \mathbf{C}_b^n \delta\boldsymbol{\omega}_{ib}^b \end{bmatrix} \tag{4}$$

where $\delta\mathbf{r}^n$, $\delta\mathbf{v}^n$ and $\boldsymbol{\psi}$ are the errors of position, velocity, and attitude. $\mathbf{C}_b^n$ is the Direction Cosine Matrix (DCM) from b-frame (i.e., the body frame) to n-frame (i.e., the navigation frame). $\mathbf{f}^n$ is the specific force vector projected to n-frame, and $\boldsymbol{\omega}_{ie}^n$ and $\boldsymbol{\omega}_{en}^n$ represent the angular rate of the Earth and that of n-frame with respect to e-frame (i.e. the Earth frame), both projected to n-frame. The symbol "×"denotes cross product of two vectors. $\delta\mathbf{f}^b$ and $\delta\boldsymbol{\omega}_{ib}^b$ are the output errors of accelerometers and gyros, as explained in (1) and (2).

C. Kalman Filter-Measurement Model

Different kinds of constraints are used to build the measurement model, including the pseudo-observations, the accelerometer and magnetometer measurements, and the quasi-static attitude updates.

1) Pseudo-Observations: The pseudo-position and pseudo-velocity observations are proposed based on the fact that the range of the position and linear velocity of the IMU are within a limited scope [16]. In this paper, we use the pseudo-position update while walking with natural human motions. The measurement model of pseudo-position is

$$\hat{\mathbf{r}}^n - \tilde{\mathbf{r}}^n = \delta\mathbf{r}^n + \mathbf{n}_1 \tag{5}$$

with $\tilde{\mathbf{r}}^n = \mathbf{constant}$

where $\hat{\mathbf{r}}^n$ and $\tilde{\mathbf{r}}^n$ are the position vectors from the INS mechanization and pseudo-position, respectively; $\delta\mathbf{r}^n$ is the position errors vector; and $\mathbf{n}_1$ is the measurement noises (i.e. the inaccuracy) of the pseudo-position.

Here is a feasible way of setting the $\mathbf{R}$ matrix for the pseudo-position: first a set of initial position noises are set roughly; then the position changes during a period can be calculated; based on this result, the elements in $\mathbf{R}$ could be further tuned. This process is done autonomously by the software.

TABLE III
ROUGH REFERENCE VALUES OF GYRO BIASES

	Phone #1	Phone #2	Phone #3
Gyro X (deg/s)	0.9	6.2	1.3
Gyro Y (deg/s)	-2.1	-2.1	-2.6
Gyro Z (deg/s)	2.8	4.0	2.0

2) Accelerometer Measurement Model: In this paper, the purpose of using accelerometers and magnetometers focuses on providing most accurate gyro bias estimation, which is different from the attitude and heading reference systems (AHRS) [20]. We build the measurement model by using the accelerometer readings directly, instead of using the accelerometers-derived roll and pitch angles. This is important for the pedestrian navigation applications with arbitrary phone displacements, since it avoids the singularity problem when the pitch angle reaches ± 90°. The tightly-coupled accelerometer measurement model is [21]

$$\delta\mathbf{f}^n = \mathbf{f}^n - \hat{\mathbf{f}}^n = \mathbf{f}^n - \hat{\mathbf{C}}_b^n \tilde{\mathbf{f}}^b \tag{6}$$

When neglecting the accelerometer deterministic errors,

$$\begin{aligned} \delta\mathbf{f}^n &= \mathbf{f}^n - \left(\mathbf{I} - [\boldsymbol{\psi}\times]\right)\mathbf{C}_b^n\mathbf{f}^b + \hat{\mathbf{C}}_b^n\mathbf{n}_2 \\ &= -[\boldsymbol{\psi}\times]\mathbf{g}^n + \hat{\mathbf{C}}_b^n\mathbf{n}_2 \\ &= [\mathbf{g}^n\times]\boldsymbol{\psi} + \hat{\mathbf{C}}_b^n\mathbf{n}_2 \end{aligned} \tag{7}$$

where, $\mathbf{f}^n = -\mathbf{g}^n = \begin{bmatrix} 0 & 0 & -g \end{bmatrix}^T$, $\hat{\mathbf{C}}_n^b$ is the DCM provided by the Kalman filter, g is the local gravity value, $\boldsymbol{\psi}$ is the attitude error, and $\mathbf{n}_2$ is the noise.

For pedestrian applications, the acceleration are commonly high-frequency and alternating. Thus, it is reasonable to model the actual accelerations as measurement noises. The components in $\mathbf{R}$ related to the accelerometer measurements are set based on the value of the actual linear acceleration A

$$A = \left| norm(\mathbf{f}^b) - g \right| \tag{8}$$

When $A \leq |Th_{acc1}|$ (i.e., in non-acceleration mode), the corresponding components in $\mathbf{R}$ are set as σ_a^2, where σ_a^2 is set according to the specifications of the accelerometer used.

When $|Th_{acc1}| \leq A \leq |Th_{acc2}|$ (i.e., in low-acceleration mode), the acceleration uncertainties is set as $s(A^2/P)\sigma_a^2$,

TABLE IV
MAGNETOMETER READINGS AND CALIBRATED LMF WHEN WALKING (HANDHELD) IN OUTDOORS AND INDOORS

	Outdoor	Indoor
Magnetometer readings	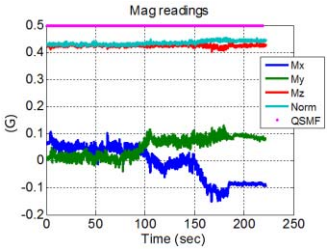	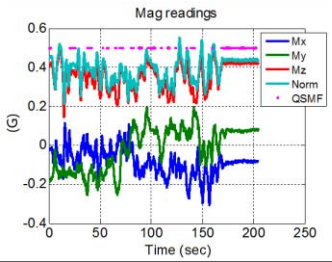
Calibrated LMF	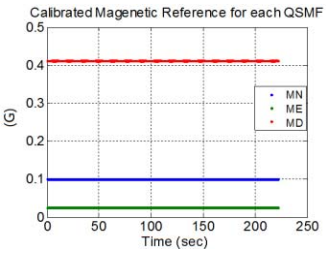	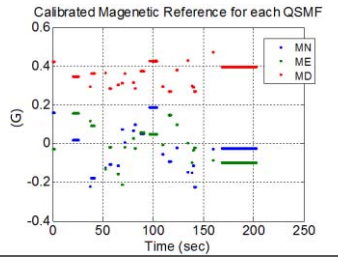

Fig. 3. Outdoor test environment and trajectory.

where P is the corresponding components of attitudes in the covariance matrix and s is a scalar. This parameter setting method follows the research in [21].

When $A \geq |Th_{acc2}|$ (i.e., in high-acceleration mode), the accelerometer is far away from the truth. Accordingly, the components in $\mathbf{R}$ are set as a large number σ^2_{aMax}. In this situation, the accelerometer measurements will not contribute to the solution.

3) Magnetometer Measurement Model: The perturbations in the magnetometer measurements are different from that in the accelerometers. The latter is commonly high-frequency and alternating; however, the magnetic perturbations are caused by external magnetic bodies such as man-made infrastructures. Therefore, a typical type of magnetic perturbation is that both the direction and strength of the LMF are changed, but the change is stable within a limited space (or periods). The period during which the LMF is stable can be called as quasi-static magnetic field (QSMF) period, and can be detected by using the magnitude of magnetometer readings [22].

In this paper, we use magnetometer measurements to improve the gyro calibration during QSMF periods. It is assumed that we have totally no idea about the LMF parameters. The details about these magnetic field parameters can refer to [23]. Instead, we calibrate the LMF at the beginning of each QSMF period. The flowchart of using magnetometers under QSMF periods is shown in Figure 1.

The LMF vector during the k-th QSMF period is calibrated by:

$$\mathbf{m}_k^n = (\hat{\mathbf{C}}_n^b)^T \tilde{\mathbf{m}}_{k,1}^b \tag{9}$$

where $\tilde{\mathbf{m}}_{k,1}^b$ is the magnetometer reading at the beginning of the first epoch(s) of k-th QSMF period. The computed $\mathbf{m}_k^n$ is then used as the reference during the k-th QSMF period.

The measurement model is built by using the magnetometer readings directly, which avoid the leveling (i.e., using the accelerometer readings to calculate the roll and pitch angles) step. Therefore, the measurement model, as shown in (10), is independent from the accelerometer measurements.

$$\delta\mathbf{m}^n = \left[\mathbf{m}^n \times\right]\boldsymbol{\psi} + \hat{\mathbf{C}}_b^n \mathbf{n}_3 \tag{10}$$

where, $\delta\mathbf{m}^n = \hat{\mathbf{C}}_b^n \tilde{\mathbf{m}}^b - \mathbf{m}^n$, $\tilde{\mathbf{m}}^b$ is the magnetometer measurement, $\mathbf{m}^n$ is the calibrated LMF vector, $\boldsymbol{\psi}$ is the attitude error, and $\mathbf{n}_3$ is the measurement noise.

4) Quasi-Static Attitude Updates: The assumption for this constraint is that any rotation sensed by the gyros should be caused by the gyro biases when the device is quasi-static. Therefore, it is feasible to improve the gyro calibration during not only strict static periods, but also any quasi-static periods such as the periods when the user stands in-situ and the phone is handheld, phoning, or putting in pocket. The detection of quasi-static periods has been detailed in [24]. The quasi-static attitude updates (QSAU) can be written as

$$\tilde{\boldsymbol{\omega}}_{ib}^b = \mathbf{b}_g + \mathbf{n}_4 \tag{11}$$

where $\tilde{\boldsymbol{\omega}}_{ib}^b$ is the output vector of a quasi-static gyro triad, $\mathbf{b}_g$ is the gyro biases, and $\mathbf{n}_4$ is the noise.

D. Parameter Setting and Initialization

The Kalman filter parameters include the initial state vector $\mathbf{x}_0$ (i.e., the vector including the error states $\delta\mathbf{r}$, $\delta\mathbf{v}$, $\boldsymbol{\psi}$,

TABLE V

FIGURES OF CALIBRATION RESULTS IN OUTDOOR TESTS (MAGENTA DOTS INDICATE THE AVAILABILITY OF MAGNETOMETER MEASUREMENTS)

	Phone #1	Phone #2	Phone #3
Handheld	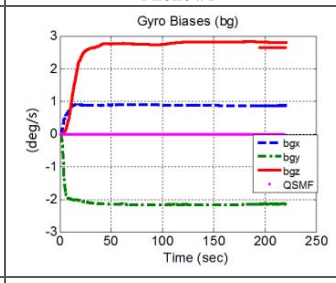	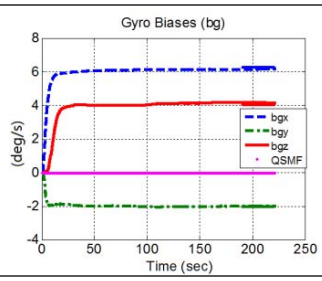	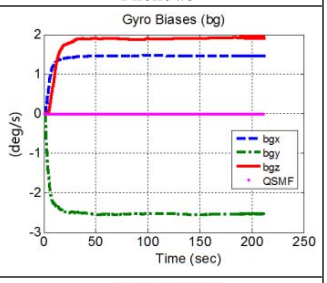
Phoning	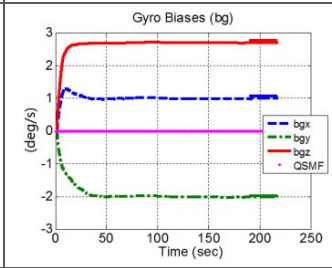	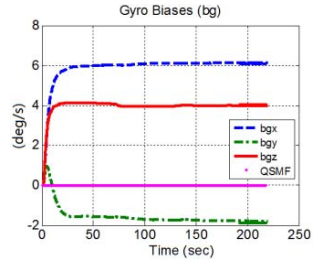	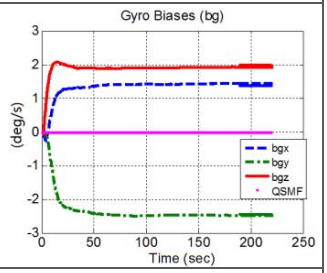
Dangling	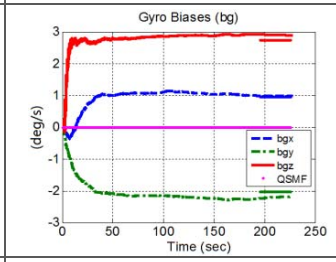	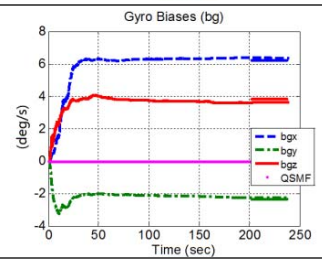	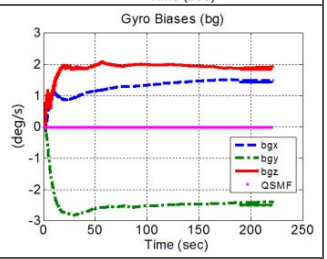
Pocket	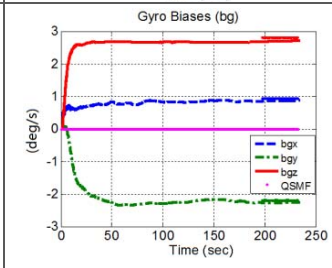	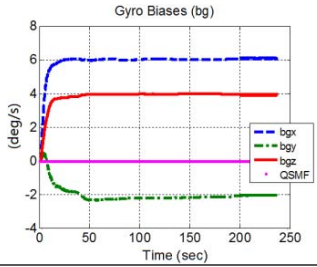	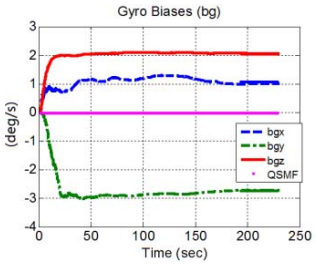
Belt	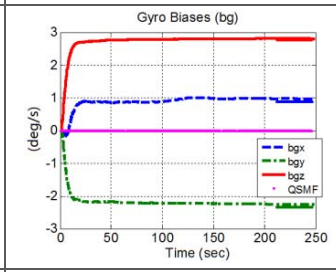	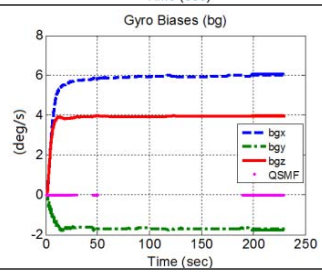	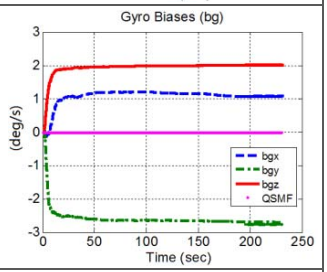
Backpack	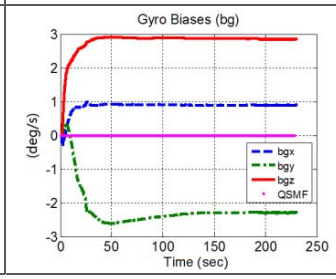	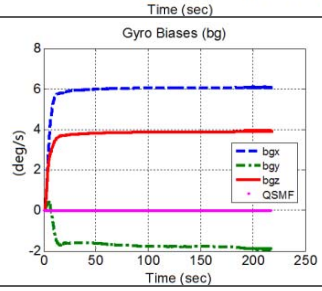	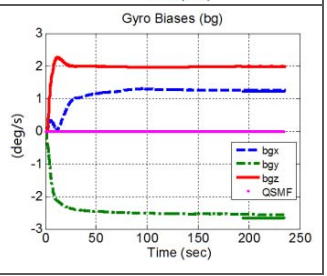

$\mathbf{b}_a$, $\mathbf{b}_g$, $\delta\mathbf{s}_a$, and $\delta\mathbf{s}_g$) and the corresponding initial values of the INS mechanization (i.e., the initial values of position $\hat{\mathbf{r}}(t_0)$, velocity $\hat{\mathbf{v}}(t_0)$, and attitude $\hat{\mathbf{C}}_b^n(t_0)$), the initial covariance matrix of state vector ($\mathbf{P}_0$), the covariance matrix of system noise ($\mathbf{Q}$) and the covariance matrix of measurement noise ($\mathbf{R}$).

TABLE VI
STATISTICAL RESULTS OF THE CALIBRATION ERRORS UNDER ALL SCENARIOS

Phone	Values (deg/s)	X	Y	Z
#1	Reference true value	0.971	-2.099	2.776
	Mean error	0.0588	0.0645	0.0845
	RMS error	0.0682	0.0843	0.0986
#2	Reference	6.173	-2.017	3.981
	Mean	0.0737	0.0655	0.0743
	RMS	0.0787	0.0752	0.0883
#3	Reference	1.291	-2.587	1.973
	Mean	0.0603	0.0583	0.0503
	RMS	0.0707	0.0645	0.0605

TABLE VII
STATISTICAL RESULTS OF THE CALIBRATION ERRORS UNDER ALL SCENARIOS

Motions	RMS error (deg/s)		
	X	Y	Z
Handheld	0.0633	0.0181	0.0589
Phoning	0.0610	0.0563	0.0643
Dangling	0.1157	0.1144	0.1230
Pocket	0.0882	0.0761	0.0815
Belt	0.0675	0.0666	0.0266
Backpack	0.0379	0.0682	0.0412

The parameters can be set as $\mathbf{x}_0 = \mathbf{0}$ (i.e., $\delta\mathbf{r} = \delta\mathbf{v} = \boldsymbol{\psi} = \mathbf{b}_a = \mathbf{b}_g = \delta\mathbf{s}_a = \delta\mathbf{s}_g = \mathbf{0}$), $\hat{\mathbf{r}}(t_0) = \mathbf{r}_0$, and $\hat{\mathbf{v}}(t_0) = \mathbf{0}$, where $\mathbf{r}_0$ is the approximate IMU position. The initial DCM $\hat{\mathbf{C}}_b^n(t_0)$ can be determined by [24]

$$\tilde{\mathbf{C}}_b^n = \left(\left[\mathbf{f}^n \ \mathbf{m}^n \ \mathbf{l}^n \right]^T \right)^{-1} \left[\tilde{\mathbf{f}}^b \ \tilde{\mathbf{m}}^b \ \tilde{\mathbf{l}}^b \right]^T \tag{12}$$

where $\mathbf{f}^n$ and $\mathbf{m}^n$ are the specific force and LMF vector in the navigation frame, $\mathbf{l}^n = \mathbf{f}^n \times \mathbf{m}^n$; $\tilde{\mathbf{f}}^b$ and $\tilde{\mathbf{m}}^b$ are the accelerometer and magnetometer measurements, and $\tilde{\mathbf{l}}^b = \tilde{\mathbf{f}}^b \times \tilde{\mathbf{m}}^b$. If the LMF is not quasi-static, the roll and pitch angles are calculated from the accelerometer measurement, and the heading angle is set as zero.

The proposed method will be tested with different smartphones under natural human motions.

IV. TESTS AND RESULTS

Different outdoor and indoor walking tests were conducted with three smartphones. The tested motion modes comprised typical phone locations and attitudes including handheld, phoning, dangling, in pocket, in belt, and in backpack. At the end of each test, there was a quasi-static period to calculate the reference values of gyro biases. The tested motion modes and the corresponding gyro and accelerometer readings are shown in Figure 2. We can see that dangling and pocket have the strongest gyro dynamics.

The tests were performed with Samsung Galaxy S3 and S4 smartphones. To make the gyro errors more significant (i.e., to test the calibration algorithm), gyro biases of 3 deg/s, −3 deg/s and 3 deg/s were added into the raw gyro outputs before data processing. The rough reference values of the gyro biases are shown in Table 3.

Fig. 4. Indoor test environment trajectory.

A. Difference Between Outdoors and Indoors

The main difference between indoor and outdoor environments is the existence of magnetic perturbations. The commonly used method of using magnetometers is straightforward and consist of three steps [25]: a) leveling the magnetometer readings by using the accelerometers; b) calculating the magnetic heading by using the leveled magnetometers; and c) calculating the true heading by a declination angle to the magnetic heading. This is based on the assumption that the LMF is simply the geomagnetic field and thus declination angle can be calculated from the IGRF model [26]. In real tests, we found that the majority of the outdoor tests met this assumption; however, in the indoor tests, the LMF could easily be different from the geomagnetic field, and might vary from point to point.

Table 4 provide a sample of the outdoor and indoor magnetic environments. All figures are plotted using the magnetic information while walking (handheld) case. The figures in the second row of the table show the magnetometer readings and their magnitudes (cyan lines). The yellow dots indicate the QSMF periods. The figures in the last row show the calibrated LMF. The LMF kept stable during this outdoor test; on the other hand, it varied significantly during the indoor test.

The outdoor and indoor tests will be given separately in the following two subsections.

B. Outdoor Walking Tests

The outdoor test environment and trajectory are shown in Figure 3. It is a sidewalk crossing different parking lots. Thus, there is no buildings within 10 meters from the sidewalk.

The figures of the calibraiton results are shown in Table 5. The first column indicates the tested motion modes, while the other three columns are the results of three phones. In each plot, the magenta dots indicate the availability of the magnetometer measurements. The pseudo-observation and accelerometer measurements were always available during these tests; therefore, the indicators for these constraints are not shown.

Most of the calibrated sensor errors have converged in the first 30 s, and all of them converged within 50 s.

TABLE VIII

FIGURES OF CALIBRATION RESULTS IN INDOOR TESTS (MAGENTA DOTS INDICATE THE AVAILABILITY OF MAGNETOMETER MEASUREMENTS)

	Phone #1	Phone #2	Phone #3
Handheld	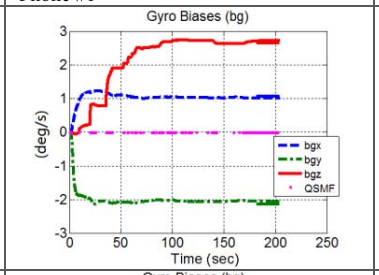	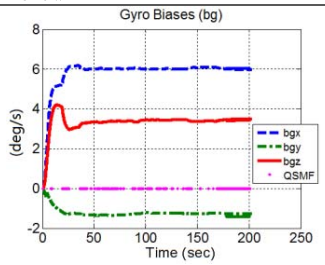	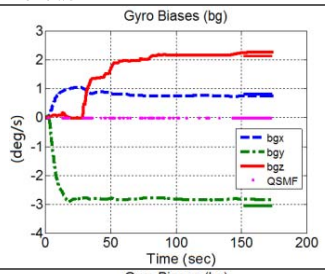
Phoning	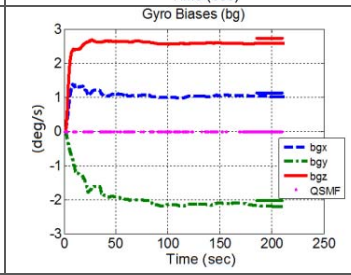	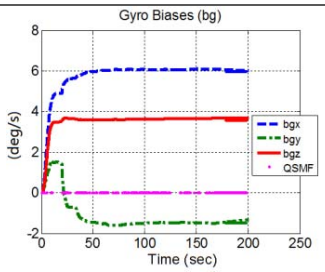	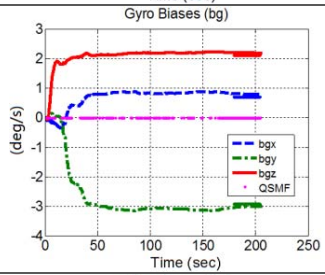
Dangling	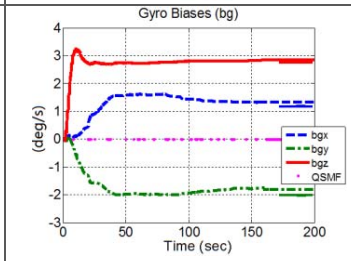	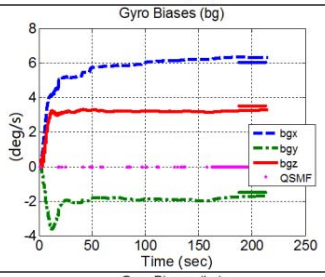	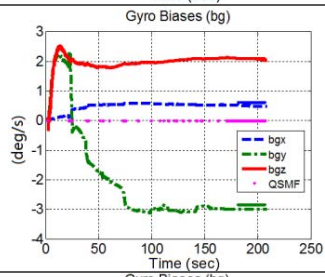
Pocket	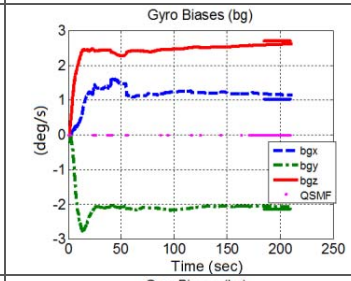	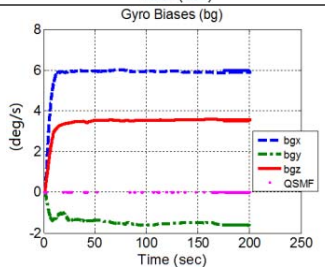	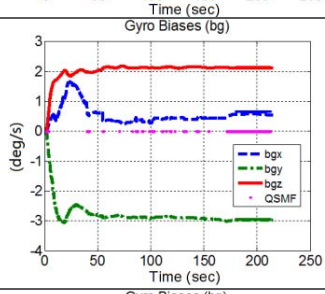
Belt	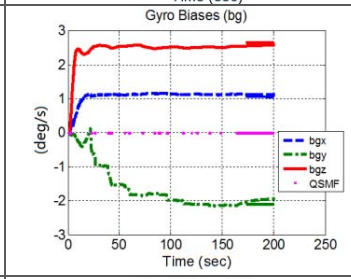	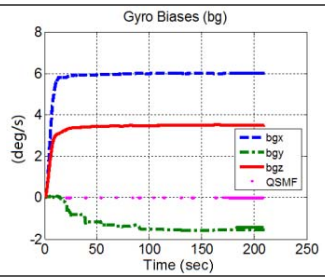	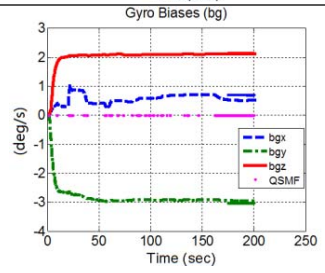
Backpack	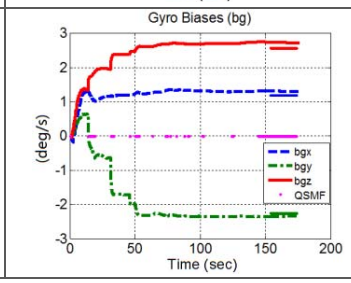	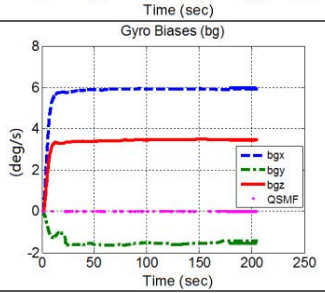	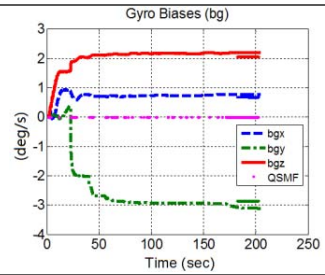

Table 6 shows the statistical results of the calibration errors under all scenarios with different phones. The mean and RMS errors were calculated using the differences between the calibration results at every epoch after convergence and the reference values obtained by averaging the gyro readings during the quasi-static periods at the end of each test.

TABLE IX
STATISTICAL RESULTS OF THE CALIBRATION ERRORS UNDER ALL SCENARIOS

Phone	Values (deg/s)	X	Y	Z
#1	Reference	1.175	-2.226	2.648
	Mean	0.0825	0.0978	0.1032
	RMS	0.0886	0.1122	0.1049
#2	Reference	6.101	-1.356	3.562
	Mean	0.0637	0.1272	0.0550
	RMS	0.0772	0.1298	0.0666
#3	Reference	0.826	-3.043	2.129
	Mean	0.1183	0.1140	0.0847
	RMS	0.1270	0.1157	0.1063

TABLE X
STATISTICAL RESULTS OF THE CALIBRATION ERRORS UNDER ALL SCENARIOS

Motions	RMS (deg/s)		
	X	Y	Z
Handheld	0.0534	0.1105	0.0786
Phoning	0.0930	0.1134	0.0920
Dangling	0.1376	0.1684	0.1462
Pocket	0.1364	0.1051	0.0789
Belt	0.0774	0.1052	0.0707
Backpack	0.0695	0.1031	0.0792

The gyro biases reduced from several deg/s to under 0.1 deg/s. Although the gyros within different phones have different biases and some are more significant (e.g., 6 deg/s in phone #2), the results are all at the same level. This indicates the possible accuracy of the calibration method.

To investigate the effect of human motions on the calibration, we also calculated the statistical results under different motion modes. The results are shown in Table 7.

Dangling and pocket have larger calibration errors than the other motions modes. This meets our expectation, since both dangling and pocket provide stronger smartphone dynamics, as shown in Figure 2. Even under such challenging conditions, the gyro biases were reduced to under 0.13 deg/s and 0.1 deg/s, respectively.

C. Indoor Walking Tests

The indoor tests were conducted at the main floor of the Energy Environment Experiential Learning (EEEL) building at the University of Calgary, which has a size of approximate 120×40 m^2. EEEL is a relatively new building with well-equipped facilities. Accordingly, the magnetic perturbations are also significant in this building, which makes it an appropriate place for the indoor tests. The test environment and trajectory are shown in Figure 4.

The result figures are shown in Table 8. The solid line at the end of each curve indicates the reference value calculated from the quasi-static data.

The discontinuity of the periods with magnetometer updates indicates the frequent magnetic perturbations indoors.

TABLE XI
FIGURES OF CALIBRATION RESULTS USING MAGNETOMETERS UNDER QSMF AND THAT TOTALLY IGNORING MAGNETOMETERS (WITH PHONE #1)

	Using magnetometers only during QSMF periods	Totally ignoring magnetometers
Handheld	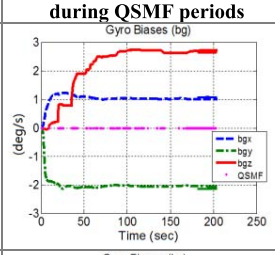	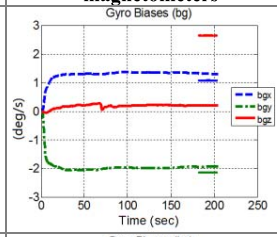
Phoning	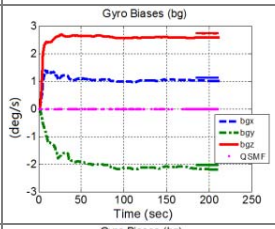	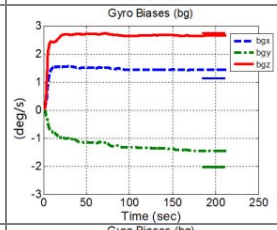
Dangling	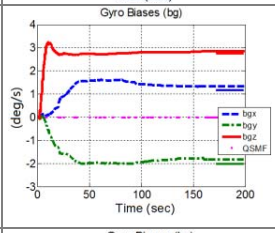	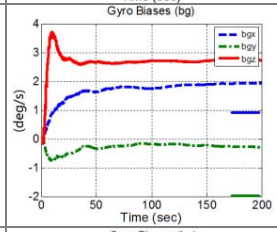
Pocket	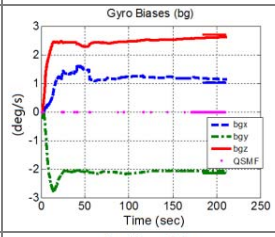	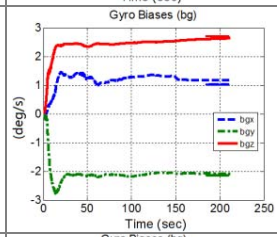
Belt	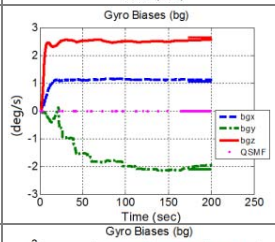	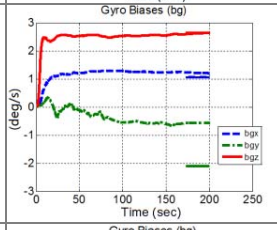
Backpack	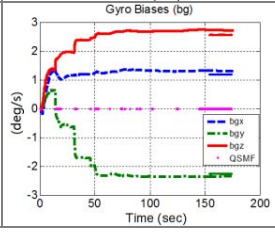	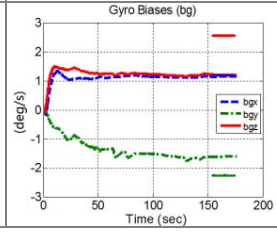

The convergence of gyro biases is not as smooth as those outdoors; however, even under such challenging environments, all the gyro biases have converged to the right values within 100 s under different human motions. This has verified the feasibility of the proposed method for pedestrian applications. Table 9 shows the statistical results of calibration errors under all scenarios with different phones, and Table 10 classifies the results by motion modes.

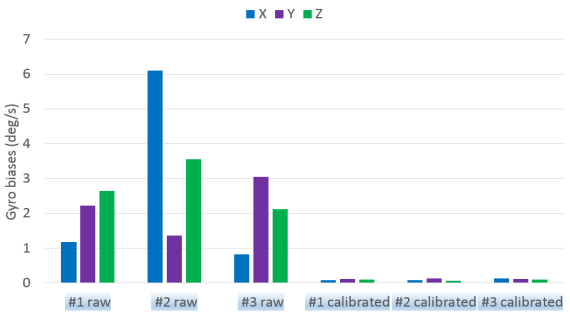

Fig. 5. Gyro biases without and with the proposed real-time calibration.

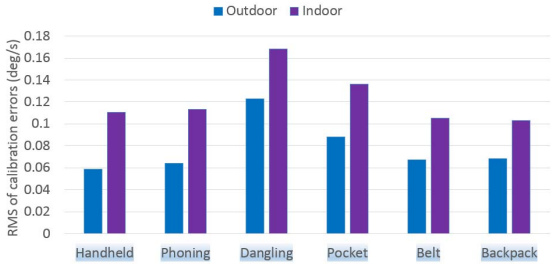

Fig. 6. Calibration errors under typical motions both indoors and outdoors.

Table 9 indicates that the proposed calibration method reduced the gyro biases from several deg/s to under 0.13 deg/s in the indoor tests, which is larger than the 0.1 deg/s outdoors. These results are promising for MEMS sensors, since the indoor environment is much harsher the outdoor. In Table 10, the largest calibration errors under dangling and pocket are 0.17 and 0.14 deg/s, which are still larger than those under other motions. The calibration errors under handheld, phoning, belt, and backpack are less than 0.12 deg/s.

Comparing with previous methods such as the vertical gyro method or the methods that use accelerometers to estimate the horizontal gyro errors, an advantage of the proposed method is to use magnetometers during QSMF periods to calibrate the vertical component of gyro biases. Natural human motion signals are usually periodic, as indicated in Figure 2; therefore, not all the gyro axis has the chance to move to the horizontal direction. Thus, the magnetometers measurements during QSMF periods is important. Table 11 show the calibration results using magnetometers measurements under QSMF and that totally ignoring magnetometers. These results further verify the effectiveness of the proposed method in calibrating the vertical gyro bias component.

D. Summary of Test Results

To make a summary, Figure 5 shows the gyro biases without and with the proposed real-time calibration. The gyro biases of tested phones were reduced from several deg/s to less than 0.15 even in indoor environments. Although the tested phones have different gyro bias values, the calibration errors are at the same level.

Figure 6 compares the calibration errors under different motion modes both indoors and outdoors. The results are better outdoors than indoors under all motion modes. This is most probably because of the harsh magnetic environment indoors. Dangling and pocket are two challenging motion modes for gyro calibration. Their calibration errors are 0.17 and 0.14 deg/s indoors, and 0.13 and 0.09 deg/s outdoors. Under other motions, i.e., handheld, phoning, belt, and backpack, the calibration errors are under 0.12 deg/s indoors and 0.07 outdoors. The calibration results are promising for low cost MEMS sensors in consumer portable devices, even when considering that a part of the calibration errors may be caused by the temperature variations of the gyro errors themselves.

V. Conclusion and Future Works

This paper proposed a real-time calibration method without external equipment and without user intervention for gyro sensors in portable devices. The method was tested under walking tests with typical human motions, including handheld, phoning, dangling, pocket, belt, and backpack, both outdoors and indoors. The gyro biases of tested smartphones were reduced from several deg/s to under 0.15 deg/s indoors and 0.1 deg/s outdoors. Under the most challenging motion modes for sensors-based pedestrian navigation, i.e., dangling and pocket, the calibration errors were 0.17 and 0.14 deg/s indoors, and 0.13 and 0.09 deg/s outdoors. Under other motions, the calibration errors are less than 0.12 deg/s indoors and 0.07 outdoors. This calibration method can work in real-time and has a potential for calibration of the MEMS gyros within consumer electronics.

Future works will focus on optimizing the proposed method, e.g., reducing the computational load and further improving the convergence rate.

References

[1] N. El-Sheimy and X. Niu, "The promise of MEMS to the navigation community," *Inside GNSS*, vol. 2, no. 2, pp. 46–56, 2007.
[2] C. Huang, Z. Liao, and L. Zhao, "Synergism of INS and PDR in self-contained pedestrian tracking with a miniature sensor module," *IEEE Sensors J.*, vol. 10, no. 8, pp. 1349–1359, Aug. 2010.
[3] Y. Zhuang, H. W. Chang, and N. El-Sheimy, "A MEMS multi-sensors system for pedestrian navigation," in *Proc. China Satellite Navigat. Conf. (CSNC)*, 2013, pp. 651–660.
[4] X. Niu, Y. Li, H. Zhang, Q. Wang, and Y. Ban, "Fast thermal calibration of low-grade inertial sensors and inertial measurement units," *Sensors*, vol. 13, no. 9, pp. 12192–12217, 2013.
[5] InvenSense. (2014). *MPU-6500 Product Specification Revision 1.1*. [Online]. Available: http://www.invensense.com/mems/gyro/mpu6500.html, accessed Nov. 20, 2014.
[6] D. Titterton and J. Weston, *Strapdown Inertial Navigation Technology*, 2nd ed. London, U.K.: IEE, 2004.
[7] Z. F. Syed, P. Aggarwal, C. Goodall, X. Niu, and N. El-Sheimy, "A new multi-position calibration method for MEMS inertial navigation systems," *Meas. Sci. Technol.*, vol. 18, no. 7, p. 1897, 2007.
[8] L. Xiao, S. Wei, and W. Sun, "Research on the high accuracy rapid test method of IMU," *J. Astron.*, vol. 29, no. 1, pp. 172–177, 2008.
[9] J. C. Lötters, J. Schipper, P. H. Veltink, W. Olthuis, and P. Bergveld, "Procedure for in-use calibration of triaxial accelerometers in medical applications," *Sens. Actuators A, Phys.*, vol. 68, nos. 1–3, pp. 221–228, Jun. 1998.
[10] I. Skog and P. Händel, "Calibration of a MEMS inertial measurement unit," in *Proc. 17th IMEKO World Congr.*, 2006, pp. 1–6.
[11] H. Zhang, Y. Wu, W. Wu, M. Wu, and X. Hu, "Improved multi-position calibration for inertial measurement units," *Meas. Sci. Technol.*, vol. 21, no. 1, p. 015107, 2010.

[12] T. Nieminen, J. Kangas, S. Suuriniemi, and L. Kettunen, "An enhanced multi-position calibration method for consumer-grade inertial measurement units applied and tested," *Meas. Sci. Technol.*, vol. 21, no. 10, p. 105204, 2010.
[13] E.-H. Shin and N. El-Sheimy, "A new calibration method for strapdown inertial navigation systems," *Zeitschrift Vermessungswesen*, vol. 127, no. 1, pp. 1–10, 2002.
[14] W. T. Fong, S. K. Ong, and A. Y. C. Nee, "Methods for in-field user calibration of an inertial measurement unit without external equipment," *Meas. Sci. Technol.*, vol. 19, no. 8, p. 085202, 2008.
[15] InertialLabs. (Mar. 2014). *Vertical Gyro System VG Interface Control Document*. [Online]. Available: http://inertiallabs.com/downloads/new/VG_ICD_rev_1.4_Mar14.pdf, accessed Jan. 19, 2015.
[16] Y. Li, X. Niu, Q. Zhang, H. Zhang, and C. Shi, "An *in situ* hand calibration method using a pseudo-observation scheme for low-end inertial measurement units," *Meas. Sci. Technol.*, vol. 23, no. 10, p. 105104, 2012.
[17] E.-H. Shin, "Estimation techniques for low-cost inertial navigation," Dept. Geomatics Eng., Univ. Calgary, Calgary, AB, Canada, Tech. Rep. UCGE 20219, 2005.
[18] R. G. Brown and P. Y. C. Hwang, *Introduction to Random Signals and Applied Kalman Filtering*, vol. 1. New York, NY, USA: Wiley, 1992.
[19] P. S. Maybeck, *Stochastic Models, Estimation, and Control*, vol. 3. Amsterdam, The Netherlands: Elsevier, 1982.
[20] W. Li and J. Wang, "Effective adaptive Kalman filter for MEMS-IMU/magnetometers integrated attitude and heading reference systems," *J. Navigat.*, vol. 66, no. 1, pp. 99–113, Jan. 2013.
[21] M. Wang, Y. Yang, R. R. Hatch, and Y. Zhang, "Adaptive filter for a miniature MEMS based attitude and heading reference system," in *Proc. IEEE Position Location Navigat. Symp. (PLANS)*, Apr. 2004, pp. 193–200.
[22] M. H. Afzal, V. Renaudin, and G. Lachapelle, "Use of earth's magnetic field for mitigating gyroscope errors regardless of magnetic perturbation," *Sensors*, vol. 11, no. 12, pp. 11390–11414, 2011.
[23] M. J. Caruso, "Applications of magnetic sensors for low cost compass systems," in *Proc. IEEE Position Location Navigat. Symp.*, Mar. 2000, pp. 177–184.
[24] A. Saxena, G. Gupta, V. Gerasimov, and S. Ourselin, "In use parameter estimation of inertial sensors by detecting multilevel quasi-static states," in *Knowledge-Based Intelligent Information and Engineering Systems*. Berlin, Germany: Springer-Verlag, 2005.
[25] R. Zhang, F. Hoflinger, and L. Reindl, "Inertial sensor based indoor localization and monitoring system for emergency responders," *IEEE Sensors J.*, vol. 13, no. 2, pp. 838–848, Feb. 2013.
[26] A. Chambodut, "Geomagnetic field, IGRF," in *Encyclopedia of Solid Earth Geophysics*. Berlin, Germany: Springer-Verlag, 2011, pp. 379–380.

You Li (S'15) is currently pursuing the Ph.D. degree with the MMSS Research Group, University of Calgary, and the GNSS Research Center, Wuhan University. He was a Software Algorithm Designer with InvenSense Inc., Canada. He has authored 15 papers in referred journals and conferences, and holds three patents. His research interests are microelectromechanical systems sensors, the multisensor integration technologies, and their applications.

Jacques Georgy (S'09–M'10) received the B.Sc. and M.Sc. degrees in computer and systems engineering from Ain Shams University, Egypt, in 2001 and 2007, respectively, and the Ph.D. degree in electrical and computer engineering from Queen's University, Canada, in 2010. He was the Vice President of Research and Development, and the Co-Founder of Trusted Positioning Inc., until it was acquired by InvenSense Inc. He is currently the Director of Navigation Research and Development with InvenSense Inc. He is involved in positioning and navigation systems for portable, vehicular, and machinery applications. He has co-authored a book, and authored or co-authored over 70 papers. He holds one issued patent, and 26 distinct patents pending. His research interests include linear and nonlinear state estimation, positioning and navigation systems, autonomous mobile robot navigation, and underwater target tracking. He was a recipient of the Institute of Navigation's Early Achievement Award for his contributions to portable and indoor navigation using microelectromechanical systems inertial sensors on consumer devices in 2013.

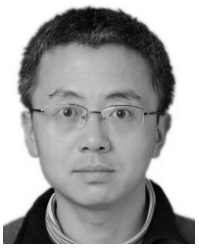

Xiaoji Niu received the bachelor's and Ph.D. degrees from the Department of Precision Instruments, Tsinghua University, in 1997 and 2002, respectively. He did post-doctoral research at the University of Calgary for four years, and was a Senior Scientist with SiRF Technology Inc., for three years. He is currently a Professor with the GNSS Research Center, Wuhan University, China. He leads the GNSS/INS Group with more than 20 members, including faculties, post-doctors, and graduate students. The group focuses on GNSS/INS deep integration, low-cost navigation sensor fusion, and their applications. He has authored over 70 academic papers, and holds nine patents.

Qingli Li received the bachelor's degree in surveying and mapping from Wuhan University, in 2014, where she is currently pursuing the master's degree at the School of Geodesy and Geomatics. Her research focuses on Global Navigation Satellite System/Inertial Navigation System integration technologies.

Naser El-Sheimy is currently a Professor and the Leader of the MMSS Research Group at the University of Calgary, and was the Chairman of Trusted Positioning Inc. He authored two books, eight book chapters, and over 400 papers in refereed journals and conferences, and holds nine patents. His area of expertise is in the integration of GNSS/INS/imaging sensors for navigation, mapping, and Geographic Information System applications with special emphasis on mobile mapping systems. He holds the Canada Research Chair in Mobile Multisensors Geomatics Systems.